Sparse and composite coherent lattices

Eric Betzig
New Millennium Research, LLC, 2174 Butternut Drive, Okemos, Michigan 48864 USA
(Received 3 January 2005; published 20 June 2005)

A method is described that yields a series of $(D+1)$-element wave-vector sets giving rise to ($D=2$ or 3)-dimensional coherent sparse lattices of any desired Bravais symmetry and primitive cell shape, but of increasing period relative to the excitation wavelength. By applying lattice symmetry operations to any of these sets, composite lattices of $N>D+1$ waves are constructed, having increased spatial frequency content but unchanged crystal group symmetry and periodicity. Optical lattices of widely spaced excitation maxima of diffraction-limited confinement and controllable polarization can thereby be created, possibly useful for quantum optics, lithography, or multifocal microscopy.

DOI: 10.1103/PhysRevA.71.063406 PACS number(s): 32.80.Pj, 61.50.Ah, 87.64.Tt

Optical lattices are spatially periodic interference patterns arising from the superposition of a finite set of plane waves. They have been harnessed in one (1D) through three dimensions (3D) for diverse applications including optical sectioning [1] and superresolution [2,3] in cellular imaging; photonic crystal lithography [4,5]; and quantum optics experiments [6–8], including the demonstration of a quantum phase transition in a lattice-confined Bose-Einstein condensate [9]. Thus far, all such applications have been limited to closely packed lattices of periodicity less than the excitation wavelength λ.

In this paper, I lift this constraint and develop the mathematical basis for two further constructs: *sparse lattices*, of many possible periods, including those large compared to λ; and *composite lattices*, containing larger sets of plane waves, and resulting in improved confinement of the excitation at discrete intensity maxima. Together, sparse composite lattices permit the creation of 2D and 3D arrays of widely spaced, and hence individually resolvable, excitation maxima of controllable polarization, with each maximum confined to near the diffraction limit in all directions. As such, they may be suitable as multifocal excitation fields for live-cell fluorescence imaging with improved spatial and temporal resolution; the fabrication of photonic crystals with specially tailored diffracting structures in each primitive cell; massively parallel two-photon absorption lithography [10] of 3D structures large compared to λ; and optical trapping of biological objects or ultracold atoms in optimally steep and symmetric potentials. The latter may lead to individually addressable atomic qubits for use in quantum computation.

As with any 2D or 3D periodic structure, optical lattices can be classified by their Bravais symmetry, and described in the same crystallographic terms used in most texts on solid-state physics [11]. In a key paper [12], this connection was made, along with three powerful observations. First, the spatial properties of the lattice, such as its symmetry, primitive cell shape, and periodicity, depend only on the wave vectors $\mathbf{k}_n$ of the plane waves and not their electric fields $\mathbf{e}_n$. Thus, the problem of finding a suitable lattice field $\mathbf{e}(\mathbf{x},t)$ for any application can be broken into two parts: finding the $\mathbf{k}_n$ that define the lattice; and finding the $\mathbf{e}_n$ that determine the basis (the field pattern that identically exists in each primitive cell) for this lattice. Second, a D-dimensional lattice ($D=2$ or 3) requires a minimum of $D+1$ wave vectors, since two wave vectors $\mathbf{k}_0,\mathbf{k}_1$ define a 1D lattice $\mathbf{e}(\mathbf{x},t)=\mathbf{e}(x,t)$, where $\hat{\mathbf{e}}_x \| (\mathbf{k}_1-\mathbf{k}_0)$, and three wavevectors $\mathbf{k}_0,\mathbf{k}_1,\mathbf{k}_2$ define a 2D lattice $\mathbf{e}(\mathbf{x},t)=\mathbf{e}(x,y,t)$, where $\hat{\mathbf{e}}_z \| (\mathbf{k}_1\times\mathbf{k}_2+\mathbf{k}_2\times\mathbf{k}_3+\mathbf{k}_3\times\mathbf{k}_1)$. Finally, the reciprocal lattice corresponding to a given D-dimensional direct (i.e., real-space) lattice comprised of $D+1$ wave vectors can be constructed from the D reciprocal primitive vectors

$$\mathbf{b}_n = \mathbf{k}_0 - \mathbf{k}_n, \quad n = 1,\ldots,D. \tag{1}$$

Since the spatial properties of sparse and composite lattices will also depend only on the wave vectors $\mathbf{k}_n$, the construction methods that follow apply to any set of coherent waves, including acoustic, interfacial (e.g., air/water), and monoenergetic matter waves. We therefore use the more general term *coherent lattice* to describe such constructs, reserving the more common expression *optical lattice* for describing the construction of the basis $\mathbf{e}(\mathbf{x},t)$ from a set of electromagnetic waves.

We can extend the observations of [12] and find a set $\{\mathbf{k}_m\}$ of $D+1$ wave vectors yielding a D-dimensional coherent lattice of any desired Bravais symmetry and Wigner-Seitz primitive cell shape by first selecting a set $\{\mathbf{a}_n\}$ of (nonunique) D primitive vectors to describe the lattice. Expressing these as column vectors, a $D\times D$ direct lattice matrix $\mathbf{A}=[\mathbf{a}_1,\ldots,\mathbf{a}_D]$ is defined. A corresponding set $\{\mathbf{b}_n\}$ of reciprocal primitive vectors is found from the relationship $\mathbf{b}'_i\cdot\mathbf{a}_j=2\pi\delta_{ij}$ arising from the definition of the reciprocal lattice [11]. Expressed in matrix form, this yields $\mathbf{B}'\cdot\mathbf{A}=2\pi\mathbf{I}$ or, equivalently,

$$\mathbf{B} \equiv [\mathrm{b}_1,\ldots,\mathrm{b}_D] = 2\pi(\mathbf{A}')^{-1} \tag{2}$$

where the prime denotes the transpose. $\mathbf{B}$ is the $D\times D$ reciprocal lattice matrix.

To find the $\{\mathbf{k}_m\}$ for a lattice defined by $\mathbf{A}$, we apply the monochromaticity condition $|\mathbf{k}_m| \equiv k = 2\pi/\lambda$ to Eq. (1), yielding $|\mathbf{k}_n|^2 = |\mathbf{k}_0-\mathbf{b}_n|^2 = k^2 - 2\mathbf{b}'_n\cdot\mathbf{k}_0 + \mathbf{b}'_n\cdot\mathbf{b}_n = k^2$ or, once again in matrix form,

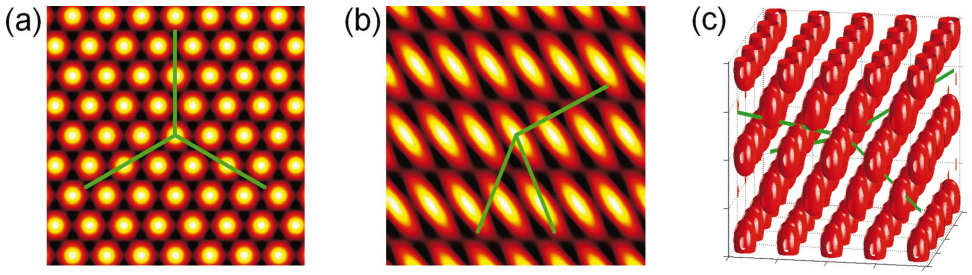

FIG. 1. (Color) Wave vectors (green) and resulting plots of $|\mathbf{e}(\mathbf{x})|^2$ over $(5\lambda)^2$ for (a) 2D hexagonal and (b) 2D oblique fundamental lattices. (c) Isosurfaces of $0.5\max(|\mathbf{e}(\mathbf{x})|^2)$ over $(6.8\lambda)^2$ for a 3D centered tetragonal fundamental lattice.

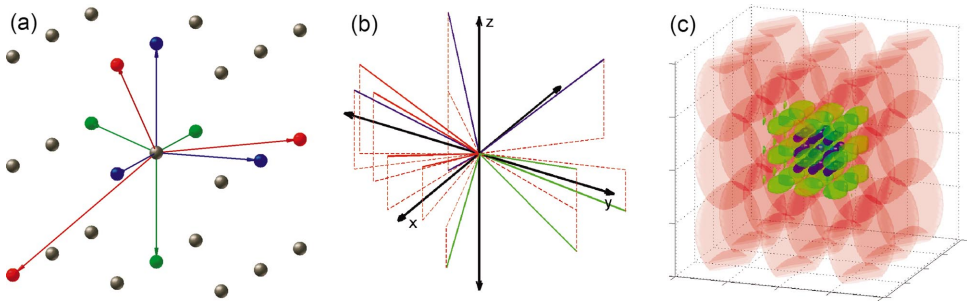

FIG. 2. (Color) (a) Direct lattice primitive vectors and resulting (b) wave vectors and (c) isosurfaces of $0.5\max(|\mathbf{e}(\mathbf{x})|^2)$ over three periods of $|\mathbf{e}(\mathbf{x})|^2$ for the simple cubic fundamental lattice (blue, period $\sqrt{3}\lambda/2$) and simple cubic sparse lattices of period $\sqrt{11}\lambda/2$ (green) and $\sqrt{59}\lambda/2$ (red).

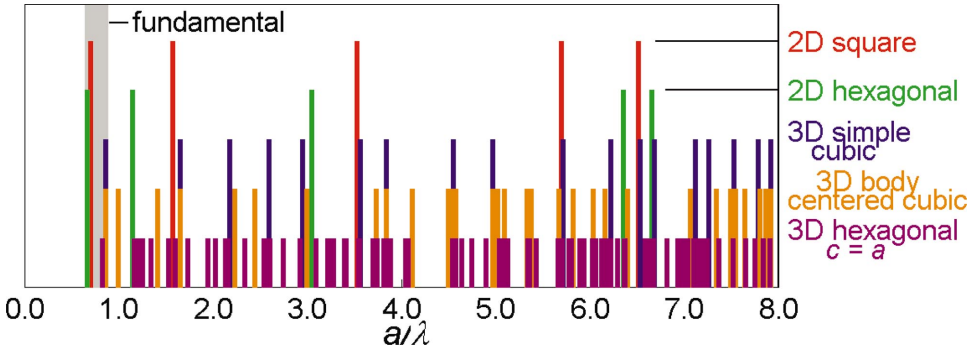

FIG. 3. (Color) Distribution of sparse lattice periodicities of $|\mathbf{e}(\mathbf{x})|^2$, as defined by the normalized conventional unit-cell lattice constant a/λ, for five lattice types.

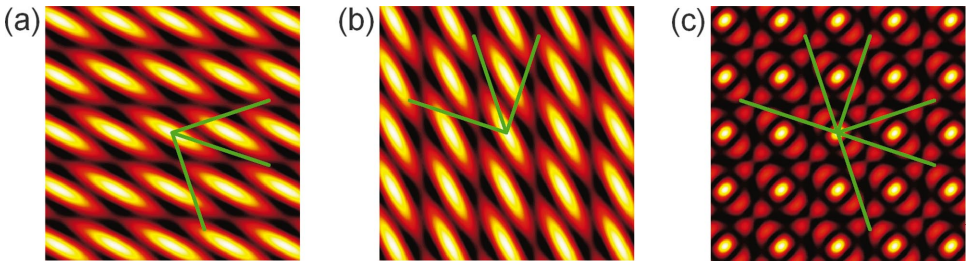

FIG. 4. (Color) (a) Wave vectors (green) and plot of $|\mathbf{e}(\mathbf{x})|^2$ for a particular 2D square sparse lattice of period $\sqrt{5/2}\lambda$. (b) Related sparse lattice obtained by rotating the wave vectors in (a) by 90°. (c) Composite lattice of improved confinement at the intensity maxima obtained by superimposing the wave vectors from (a) and (b).

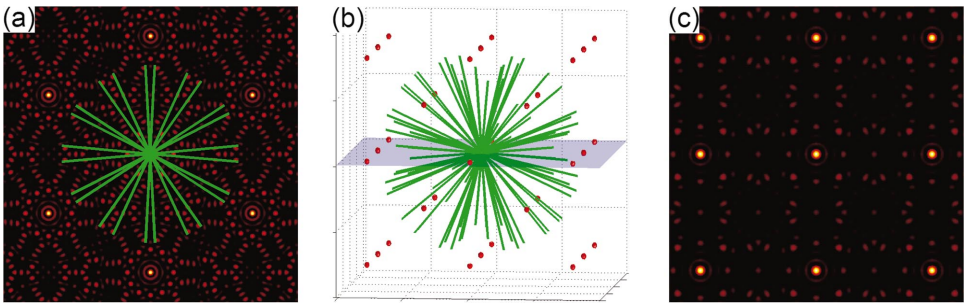

FIG. 5. (Color) Maximally symmetric composite lattices of $|\mathbf{e}(\mathbf{x})|^2$: (a) 2D hexagonal, period $\sqrt{485}\lambda/2$ (24 wave vectors); (b) 3D body-centered cubic, period $\sqrt{62}\lambda$ (96 wave vectors), isosurfaces of $0.5\max(|\mathbf{e}(\mathbf{x})|^2)$. (c) Plot of $|\mathbf{e}(\mathbf{x})|^2$ in the *xy* plane (blue) in (b), indicating the contrast of the excitation maxima with respect to the remainder of each primitive cell.

$$\mathbf{B}' \cdot \mathbf{k}_0 = [\mathbf{b}'_1 \cdot \mathbf{b}_1, \ldots, \mathbf{b}'_D \cdot \mathbf{b}_D]'/2 \equiv \boldsymbol{\beta}/2. \tag{3}$$

Combining this result with Eq. (2) leads to an expression for the first wave vector:

$$\mathbf{k}_0 = \mathbf{A} \cdot \boldsymbol{\beta}/4\pi, \tag{4}$$

while the remaining D wave vectors in $\{\mathbf{k}_m\}$ are found from this equation and Eq. (1). Wave-vector sets $\{\mathbf{k}_m\}$ and resulting coherent lattices with the symmetry of any of the five 2D or 14 3D Bravais lattices can be found in this manner, with examples shown in Fig. 1.

A key discovery is that, when different valid primitive vector sets $\{\mathbf{a}_n\}$ are initially chosen (i.e., those whose integer combinations span the entire lattice), a series of coherent lattices arise of identical symmetry and primitive cell shape, but differing λ-normalized periodicity. An example showing three such sets $\{\mathbf{a}_n\}$, corresponding wave-vector sets $\{\mathbf{k}_m\}$, and their resulting lattices is given in Fig. 2.

One manifestation of the diffraction limit is that no lattice can have a spatial frequency greater than $2k$. Therefore, in such a series, there will always be a lattice of minimum period, termed the *fundamental lattice* [e.g., the blue lattice in Fig. 2(c)]. Lattices of period larger than the fundamental lattice comprise the sparse lattices mentioned earlier. New primitive vector sets $\{\mathbf{a}_n\}_{\mathrm{II}}$ leading to their creation can be found from a known set $\{\mathbf{a}_n\}_{\mathrm{I}}$ as follows. Since the vectors in each set span the same lattice, they can be expressed as integer combinations of one another. In matrix form, this implies

$$\mathbf{A}'_{\mathrm{II}} = \mathbf{G}\mathbf{A}'_{\mathrm{I}} \text{ and } \mathbf{A}'_{\mathrm{I}} = \mathbf{H}\mathbf{A}'_{\mathrm{II}} \tag{5}$$

where $\mathbf{A}_{\mathrm{I}}, \mathbf{A}_{\mathrm{II}}$ are the direct lattice matrices associated with $\{\mathbf{a}_n\}_{\mathrm{I}}, \{\mathbf{a}_n\}_{\mathrm{II}}$, and $\mathbf{G}$ and $\mathbf{H}$ have $D \times D$ integer elements. From Eqs. (5), $\mathbf{G}^{-1} = \mathbf{H}$. Hence, $\mathbf{G}^{-1}$ also has integer elements. Thus, $|\mathbf{G}|$ and $|\mathbf{G}^{-1}|$ must be integers. However, since $|\mathbf{G}^{-1}| = 1/|\mathbf{G}|$ (true for any square matrix), we conclude that

$$|\mathbf{G}| = \pm 1. \tag{6}$$

Thus, new *generating matrices* $\mathbf{G}$, giving rise via Eq. (5) to new direct lattice matrices $\mathbf{A}_{\mathrm{II}}$ and related sparse lattices of possibly differing periodicity, can be found by cycling through different possible combinations of integer elements g_{ij} and identifying those for which Eq. (6) is satisfied. Any given $\mathbf{G}$ can be used to generate new matrices $\mathbf{A}_{\mathrm{II}}$ from a known $\mathbf{A}_{\mathrm{I}}$ associated with any Bravais symmetry. Furthermore, $|\mathbf{G}_1\mathbf{G}_2| = |\mathbf{G}_1||\mathbf{G}_2|$, so by Eq. (6), any multiplicative combination of generating matrices and their inverses is also a generating matrix.

The distribution of sparse lattice periodicities found in this manner with $a \leqslant 8\lambda$ is plotted in Fig. 3 for five Bravais lattice types. The density of solutions is largest for 3D lattices, but even 2D lattices offer several possible sizes in this range. However, although sparse lattices comprised of $D+1$ wave vectors can be created at periodicities much greater than λ, they exhibit increasingly poor confinement of the excitation with increasing size [as evident from the green and red lattices in Fig. 2(c)], since they contain only one spatial frequency in each of the $D+1$ directions defined by the possible combinations of D wave vectors from the $(D+1)$-element set.

Consequently, to create a lattice of both large λ-normalized periodicity and confinement of the excitation to significantly less than λ in all directions at each of the intensity maxima therein, additional coherent waves must be superimposed with the $D+1$ waves of a known sparse lattice of desired symmetry and periodicity in a manner that does not adversely affect these properties. Such composite lattices of $N > D+1$ coherent waves can be created, as shown in the example in Fig. 4, by applying one or more symmetry operations that map the lattice onto itself to the wave vectors of the original lattice, and then superimposing the resulting new set of wave vectors on the original one. This process can then be repeated with additional self-mapping symmetry operations to further increase the spatial frequency content of the lattice and the confinement at the individual excitation maxima therein.

Clearly then, the most tightly confined and symmetric excitation maxima within each primitive cell of a given Bravais lattice will occur for the *maximally symmetric composite lattice* comprised of all wave vectors obtained by applying all valid combinations of symmetry operations to the wave-vector set of an initial sparse lattice of the same Bravais symmetry. Since the 2D square, 2D hexagonal, and 3D lattices of the cubic crystal group have the highest symmetry, they can result in sparse, maximally symmetric composite lattices of particularly well-confined, widely separated excitation maxima, as shown in the examples in Fig. 5. As mentioned above, such lattices may prove useful for multifocal microscopy, spectroscopy, lithography, and quantum optics.

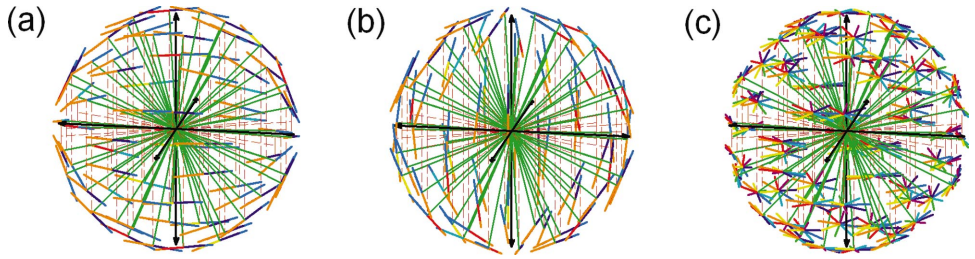

FIG. 6. (Color) 72 wave vectors (green) and corresponding electric field vectors (multiple colors) at eight times over one oscillation cycle for bases that optimize the (a) x component; (b) z component; and (c) right circular component of the total lattice field at each of the excitation maxima of the same maximally symmetric simple cubic lattice of period $\sqrt{59}\lambda/2$.

Also as mentioned above, the methods described thus far can be applied to any type of coherent waves. However, for the specific case of optical lattices comprised of electromagnetic plane waves, there still remains the issue of determining the complex electric field $\mathbf{e}_n$ of each constituent wave and resulting total basis field $\mathbf{e}(\mathbf{x},t)$ that identically exists within each primitive cell of a given lattice. Once the lattice and its set $\{\mathbf{k}_n\}$ of $N+1$ wave vectors is determined, a general approach would be to optimize a desired basis property $\Upsilon = \Upsilon(\mathbf{e}_0, \mathbf{e}_1, \ldots, \mathbf{e}_N)$, treated as a function of the plane-wave fields $\mathbf{e}_n$, and subject to the constraint that the waves are transverse, i.e., $\mathbf{k}_n \cdot \mathbf{e}_n = 0 \ \forall \ n$. A simpler yet still effective prescription, however, that leads to bases of highly confined excitation maxima of controllable polarization, is to maximize the projection of each complex plane-wave field $\mathbf{e}_n(\mathbf{x},t)$ onto a desired state $\mathbf{e}_d$ of the total lattice field $\mathbf{e}(\mathbf{x},\mathbf{t})$ at a desired position $\mathbf{x}_d$ and time t_d. Since the physical electric field is given by the real part of the complex field, the physical projection of $\mathbf{e}_n(\mathbf{x},t)$ onto $\mathbf{e}_d$ at $\mathbf{x}_d$ and t_d is given, through analogy to the bra $\langle$ ket notation of quantum mechanics, by $\mathrm{Re}\{\mathbf{e}_n^*(\mathbf{x}_d,t_d)' \cdot \mathbf{e}_d\}$. If we additionally define $\mathbf{e}_d$ in reference to some unit vector $\hat{\mathbf{e}}_p$ (e.g., $\mathbf{e}_d \| \hat{\mathbf{e}}_p$ for linear polarization, $\mathbf{e}_d \perp \hat{\mathbf{e}}_p$ for circular polarization), then $\mathbf{k}_n$ and $\hat{\mathbf{e}}_p$ define a natural orthonormal coordinate system:

$$\hat{\mathbf{e}}_{kn} \| \mathbf{k}_n, \quad \hat{\mathbf{e}}_{pk\perp n} \| (\hat{\mathbf{e}}_p \times \hat{\mathbf{e}}_{kn}), \quad \hat{\mathbf{e}}_{k\perp n} = \hat{\mathbf{e}}_{kn} \times \hat{\mathbf{e}}_{pk\perp n} \tag{7}$$

in which $\mathbf{e}_n(\mathbf{x},t)$ can be expressed as

$$\mathbf{e}_n(\mathbf{x},t) = e_n[\cos\chi \exp(i\theta)\hat{\mathbf{e}}_{k\perp n} + \sin\chi \exp(i\psi)\hat{\mathbf{e}}_{pk\perp n}]\exp[i(\mathbf{k}_n \cdot \mathbf{x} - \omega t)]. \tag{8}$$

The unknowns χ, θ, ψ are then found, thereby determining the plane-wave field $\mathbf{e}_n(\mathbf{x},t)$, by applying to $\mathrm{Re}\{\mathbf{e}_n^*(\mathbf{x}_d,t_d)' \cdot \mathbf{e}_d\} \equiv G(\chi,\theta,\psi)$ the maximization conditions $\partial G/\partial\chi = \partial G/\partial\theta = \partial G/\partial\psi = 0$, $\partial^2 G/\partial\chi^2 < 0$, $\partial^2 G/\partial\theta^2 < 0$, and $\partial^2 G/\partial\psi^2 < 0$. For example, optimizing linear polarization ($\mathbf{e}_d = E_d\hat{\mathbf{e}}_p$), we find

$$\mathbf{e}_n = e_n\hat{\mathbf{e}}_{k\perp n}\exp[-i(\mathbf{k}_n \cdot \mathbf{x}_d - \omega\mathbf{t}_d)], \tag{9}$$

and optimizing circular polarization [$\mathbf{e}_d = E_d\hat{\mathbf{e}}_R$, where $\hat{\mathbf{e}}_R \equiv (\hat{\mathbf{e}}_{pk\perp n} - i\hat{\mathbf{e}}_{p\perp n})/\sqrt{2}$ and $\hat{\mathbf{e}}_{p\perp n} \equiv \hat{\mathbf{e}}_{pk\perp n} \times \hat{\mathbf{e}}_p$] we find

$$\mathbf{e}_n = e_n \frac{-i(\hat{\mathbf{e}}_p \cdot \hat{\mathbf{e}}_{kn})\hat{\mathbf{e}}_{k\perp n} + \hat{\mathbf{e}}_{pk\perp n}}{\sqrt{1 + (\hat{\mathbf{e}}_p \cdot \hat{\mathbf{e}}_{kn})^2}}\exp[-i(\mathbf{k}_n \cdot \mathbf{x}_d - \omega\mathbf{t}_d)]. \tag{10}$$

Figure 6 shows the plane-wave electric field vectors $\mathbf{e}_n(\mathbf{x}_d,t)$ at eight times $t_q = t_d + 2\pi q/8$, $q = 0,\ldots,7$, over one oscillation cycle that arise when this procedure is used to optimize three different polarization states at the excitation maxima of the same lattice.

Maximally symmetric lattices of the cubic crystal group with bases such as these offer superior excitation confinement at discrete points compared to single-focus methods such as confocal microscopy [Figs. 7(a) and 7(b)]. Furthermore, the improved confinement and symmetric wave-vector distribution lead to steeper, more symmetric optical trapping potentials [Figs. 7(c) and 7(d)], due to the correspondingly sharper intensity gradients and cancellation of scattering forces.

Of course, the unavoidable corollary is that the experimental generation of such lattices requires careful control of the phase and propagation direction of each plane wave in a

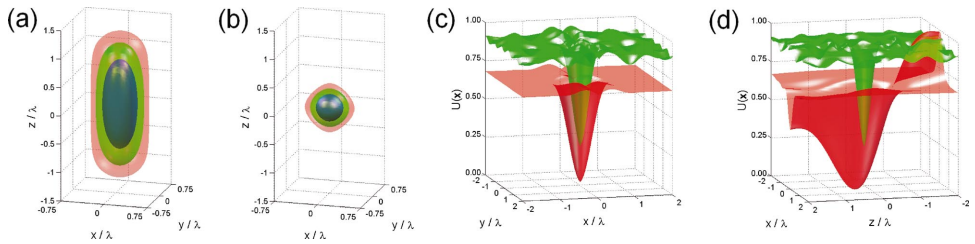

FIG. 7. (Color) (a),(b) Isosurfaces of 50% (blue), 25% (green), and 12.5% (red) of $\max(|\mathbf{e}(\mathbf{x})|^2)$ at (a) the focus of a confocal microscope (calculated via [13]); and (b) a single excitation maximum within a maximally symmetric composite body-centered cubic lattice of period $\sqrt{26}\lambda$. (c),(d) Optical trapping potential $U(\mathbf{x})$ in the (c) xy and (d) xz planes for a dielectric particle ($n = 1.6$, $ka = 0.8$ in H_2O, calculated via [14]) for the confocal (red) and lattice (green) cases considered in (a),(b).

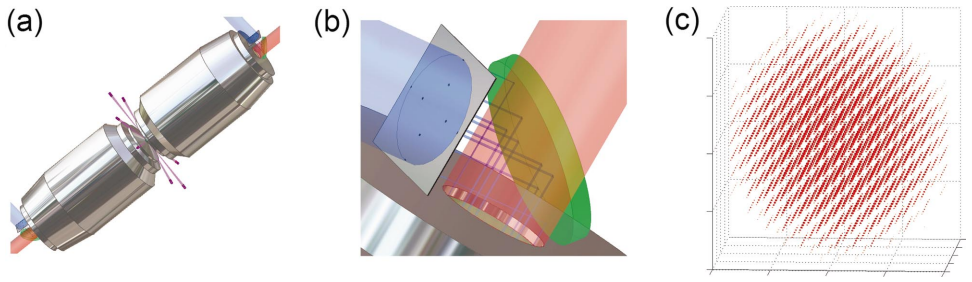

FIG. 8. (Color) Proposed experimental method: (a) opposed microscope objectives deliver multiple converging beams to a common focus; (b) said beams being created via illumination through an appropriate pupil filter at the rear of each objective. The resulting lattice [isosurfaces of $0.5\max(|\mathbf{e}(\mathbf{x})|^2)$ in (c)] is then bound to an excitation zone of controllable extent.

potentially large set. Simulations indicate that, for normally distributed phase errors among all waves, the basis does not become significantly perturbed until the mean error of each wave exceeds $\sim\lambda/5$. As detailed in [15] and summarized in Fig. 8, control at this level or better can be achieved by replacing each wave with a convergent beam propagating in the same direction $\mathbf{k}_n$ as the wave, created by illuminating the rear pupil of a high-numerical-aperture (NA) microscope objective with a confined, collimated beam located at an appropriate offset position. Many beams of a given lattice can then be created simultaneously by passing a single flat-phase beam through an aperture mask or, more flexibly, a spatial light modulator, prior to insertion at the rear pupil [Fig. 8(b)] of one of two opposed objectives [Fig. 8(a)]. Since each objective transforms a planar wave front to a spherical one, the convergent beams so defined will maintain the phase relationship necessary to produce a *bound lattice* [Fig. 8(c)] of the desired properties, confined to an *excitation zone* near the common focal point, of extent inversely proportional to the diameter of each input beam. Other beams [purple, Fig. 8(a)] from within the maximally symmetric composite set can also be optionally added with individual low-NA lenses between the objectives, thereby improving the confinement at each lattice excitation maximum. Use of opposed high-NA objectives also leads to efficient collection of the resulting signal [red in Figs. 8(a) and 8(b)] in microscopy, spectroscopy, and quantum optics applications. Finally, two groups of input beams of orthogonal polarization and controllable amplitude and phase can be combined prior to rear pupil insertion to match the field of each convergent beam to the polarization $\mathbf{e}_n$ of the corresponding plane wave, thereby controlling the ultimate basis field $\mathbf{e}(\mathbf{x},t)$.

[1] B. Bailey *et al.*, Nature (London) **366**, 44 (1993).
[2] M. G. L. Gustafsson, J. Microsc. **198**, 82 (2000).
[3] J. T. Frohn, H. F. Knapp, and A. Stemmer, Proc. Natl. Acad. Sci. U.S.A. **97**, 7232 (2000).
[4] V. Berger, O. Gauthler-Lafaye, and E. Costard, J. Appl. Phys. **82**, 60 (1997).
[5] M. Campbell *et al.*, Nature (London) **404**, 53 (2000).
[6] P. S. Jessen *et al.*, Phys. Rev. Lett. **69**, 49 (1992).
[7] A. Hemmerich and T. W. Hänsch, Phys. Rev. Lett. **70**, 410 (1993).
[8] G. Grynberg *et al.*, Phys. Rev. Lett. **70**, 2249 (1993).
[9] M. Greiner *et al.*, Nature (London) **415**, 39 (2002).
[10] T. Tanaka, H. B. Sun, and S. Kawata, Appl. Phys. Lett. **80**, 312 (2002).
[11] N. W. Ashcroft and N. D. Mermin, *Solid State Physics* (Saunders College, Philadelphia, 1976), Chaps. 4 and 5.
[12] K. I. Petsas, A. B. Coates, and G. Grynberg, Phys. Rev. A **50**, 5173 (1994).
[13] B. Richards and E. Wolf, Proc. R. Soc. London, Ser. A **253**, 358 (1959).
[14] Y. Harada and T. Asakura, Opt. Commun. **124**, 529 (1996).
[15] E. Betzig, Opt. Express **13**, 3021 (2005).